International Journal on Recent and Innovation Trends in Computing and Communication
ISSN: 2321-8169 Volume: 11 Issue: 10
DOI: https://doi.org/10.17762/ijritcc.v11i10.8520
***Article Received:** 04 August 2023 **Revised:** 30 September 2023 **Accepted:** 15 October 2023*

A Novel Hybrid CNN Denoising Technique (HDCNN) for Image Denoising with Improved Performance

Mareeswari. V[1], Nirmala.S[2]. Shashishankar.A[3], Amutha.R[4], N. Sivakumar[5], T. Jarin[6*]

[1]Department of Computer Science and Engineering. AMC Engineering College, Bengaluru, Karnataka, India. mareesh.prasanna@gmail.com, 0000-0002-6727-7034.

[2]Department of Computer Science and Engineering. AMC Engineering College, Bengaluru, Karnataka, India., drnirmala.sundaram@amceducation.in, 0009-0003-8036-4268.

[3]Department of Civil Engineering. AMC Engineering College, Bengaluru, Karnataka, India. hodcivil@amceducation.in.

[4]Department of Information Science and Engineering. AMC Engineering College, Bengaluru, Karnataka, India, amutha.shruthi@gmail.com,0000-0002-0778-7120.

[5]Department of Mechanical Engineering. AMC Engineering College, Bengaluru, Karnataka, India, nsivakumar767@gmail.com, 0000-0002-6876-3253.

[*6]Department of Electrical and Electronics Engineering, Jyothi Engineering College, Thrissur, Kerala, India, jeroever2000@gmail.com.

Abstract: Photo denoising has been tackled by deep convolutional neural networks (CNNs) with powerful learning capabilities. Unfortunately, some CNNs perform badly on complex displays because they only train one deep network for their image blurring models. We recommend a hybrid CNN denoising technique (HDCNN) to address this problem. An HDCNN consists of a dilated interfere with, a RepVGG block, an attribute sharpening interferes with, as well as one inversion. To gather more context data, DB incorporates a stretched convolution, data sequential normalization (BN), shared convergence, and the activating function called the ReLU. Convolution, BN, and reLU are combined in parallel by RVB to obtain complimentary width characteristics. The RVB's refining characteristics are used to refine FB, which is then utilized to collect more precise data. To create a crisp image, a single convolution works in conjunction with a residual learning process. These crucial elements enable the HDCNN to carry out visual denoising efficiently. The suggested HDCNN has a good denoising performance in open data sets, according to experiments.

Keywords: Image denoising, RepVGG block, HDCNN, Refining features, Deep convolutional neural networks.

I. INTRODUCTION

In order to recover a clean image x, rendering images techniques commonly construct deterioration modelling using the formula y = x v, where y stands for a specific chaotic picture and v for an additive white Gaussian noise with a normal distribution. Thus, the two categories of traditional picture denoising techniques are geographical component information approaches utilizing adjustments and altering subdomain techniques. In particular, filters (i.e., linear and nonlinear filters) are frequently used in the aforementioned spatial pixel feature techniques to decrease noise and provide a latent clean image. In addition, priori knowledge, Markov approaches, and changing domain methods were successful for picture denoising. Although these techniques have shown good results in terms of denoising, they are constrained by the following factors. To improve the performance of denoising, they first need manual parameter selection. Second, to enhance the results of image denoising, they relied on sophisticated optimization algorithms. [1]

Convolutional neural networks (CNNs) in particular were black boxes that may gathers data required for photo whitening. To solve the issue of denoising in pictures, for example, a blurring CNN (DnCNN) included sequential normalization (BN) and the activation method of ReLU. Loud maps and noisy pictures are divided into patches and fed into a deep network to train a denoiser in order to lower the price of computing. A robust denoiser is trained using two subnetworks that extract complementary features, which increases the impact of denoising. In terms of picture denoising, these CNNs have done well. They also demonstrate how several elements might be helpful for image denoising. That inspired us to design a hybrid CNN denoising system (HDCNN). [2]

International Journal on Recent and Innovation Trends in Computing and Communication
ISSN: 2321-8169 Volume: 11 Issue: 10
DOI: https://doi.org/10.17762/ijritcc.v11i10.8520
***Article Received:** 04 August 2023 **Revised:** 30 September 2023 **Accepted:** 15 October 2023*

A dilated block (DB), a RepVGG block (RVB), a feature refinement block (FB), and a single convolution make up an HDCNN. In order to give more context information, DB combines a stretched convergence, BN, ubiquitous convergence, and the activation feature of ReLU. To extract complementary width features, RVB combines convolution, BN, and reLU in parallel. Using the refining features gathered from the RVB, FB is used to gather more exact data. [3]

Noise severely impairs the ability to classify images since it changes the initial forms of the things in the picture making it challenging to use filters in real-world applications. These algorithms experience quality degradation if the simulated visual includes noise, in contrast to the human visual system, which can distinguish objects despite some degree of image disturbance. DNN-based techniques performed better than others in classifying images, however when classifying noisy images, they perform worse. Working with noiseless photographs is, however, completely impractical in real-world situations. Noise is a common cause of digital image deterioration throughout the acquisition and transition stages. [4]

When used in real-world applications, DNN-based models' accuracy noticeably declines because they are trained to operate on noiseless images. The DNN-based models' affinity for the training data is the key factor at play in this incident's occurrence. These models frequently misclassify when the test data is highly noisy and distorted.[5]

Deep learning approaches are being developed to solve the challenges mentioned. Convolutional neural networks in particular, a type of deep learning technology, are frequently used in picture denoising because of its robust learning capacity and quick execution speed. Multi-level features can be mined using a recursive unit and a gate unit to increase the memory capacity of network for picture restitution. All the algorithms can effectively denoise images, but they run the risk of making training difficult since convolutional processes change the distributions of training data.[6]

II. RELATED WORKS

Compressor Transmitter and Convolutional Detector System served as the foundation for Mo Zhao et al.'s (TECDNet) hybrid denoising solution. To increase the representational capacity of the entire model, a converter based on the Amplifier centered on innovative radial base function (RBF) attentiveness is utilized. The HSI denoising transformer (Hider), developed by Hongyu et a efficient, was suggested for the reduction of mixed HSI noise [8]. For multiscale feature aggregation, a U-shaped 3-D transformer architecture is first constructed. The spectrum transformer block also includes a multiheaded global spectral attention module that is made to dig up data in various spectral patterns.

Model-based space-variant total variation (TV) regularization is utilized for denoising with hyperparameters computed locally using a Convolutional Neural Network (CNN) with a basic and light architecture, according to the hybrid approach given by Rim et al. [9]. Madhura and others,[10] It is difficult to simultaneously collect matched information such as corrupted pictures and their equal cleaner photographs, in the underwater environment. Deep learning-based image enhancement methods frequently train their models using pairs of data.

A innovative, integrated framework for low-light picture augmentation, image denoising, and image super-resolution is put out by Jiachen et al.,[11]. A residual hybrid attention block (RHAB), the central component of this architecture, is made up of numerous dynamic down-sampling modules (DDM) and hybrid attention up-sampling modules (HAUM). A voxel-wise hybrid residual MLP-CNN model was proposed by Haibo et al. [12] to denoise three-dimensional (3D) MR images with tiny lesions. To acquire an acceptable inherent bias for the picture denoising, we combine the fundamental deep learning architectures MLP and CNN. We also integrate each output layer in MLP and CNN by adding residual connections to take advantage of distant information.

A potent HSI denoising algorithm called the NL-3DCNN, developed by Zhicheng et al. [13], combines deep learning and conventional machine learning methods. NL-3DCNN uses subspace representation to take advantage of an HSI's high spectral correlation, and the resulting representation coefficients are known as eigen images. In order to efficiently use prior knowledge about an HR-HS picture and spatial detail information in a guide image, Saori et al.'s[14] suggested estimation problem adopts hybrid spatiospectral total variation as regularization and analyzes the edge similarity between HR-HS and guide images.

By fusing the benefits of a leftover technique with a layered neural analysis-based dense encoding device, Yanqin et al. demonstrated their straightforward but efficient LDCT removing images model (CASE). In order to accurately capture and express systematic picture attributes, we built an array of CASE and a CASE-net, both of which were designed after convolutional sparse coding (CSC). Due to its high peak ratio of signal to noise (PSNR) of 23.879 dB, high second-derivative-like indicator of enhanced (SDME), high structurally indicator resemblance (SSIM), and high Precision Protect Score (EPI) of 1.045, the FAL algorithm suggested by Dinesh Kumar et al. outperformed previous approaches.

International Journal on Recent and Innovation Trends in Computing and Communication
ISSN: 2321-8169 Volume: 11 Issue: 10
DOI: https://doi.org/10.17762/ijritcc.v11i10.8520
***Article Received:** 04 August 2023 **Revised:** 30 September 2023 **Accepted:** 15 October 2023*

According to Hirald et al.,[17] the input medical images are obtained from a fresh Pap smear dataset, and after that, an image normalization approach is used to enhance the medical images' visible quality. Additionally, the hybrid feature extraction of color and texture feature vectors is carried out using a histogram of directed gradients and a modified local binary pattern, which greatly lowers the semantic gap between the feature vectors. Shuli et al.'s[18] adaptive weighted median filter image denoising approach is based on a hybrid genetic algorithm, and it addresses the issue that the classic weighted median filter has low contrast and fuzzy boundary.

For the purpose of detecting brain tumors, Balamurugan et a hybrid deep convolutional neural network (DCNN) with improved LuNet classifier algorithm has been proposed [19]. The major goal of the suggested method is to identify the tumor and categorize brain tumors as either gliomas or meningiomas. A novel hybridized deep learning framework (EN-CNN) was introduced by Gyoung et al. [20] for the reduction of picture noise from heterogeneous sources. En-CNN is primarily utilized to benchmark natural images that have additive white gaussian noise (AWGN) and impulsive noise in it (IN).

The heuristic method for lung cancer nodule identification was demonstrated by Pawar et al.,[21] and is primarily categorized as the following: image enhancement, segmenting ROI (Region of Interest), features extraction, and nodule classification. Sebastien et al [22] demonstration that a DCT denoiser can be thought of as a shallow CNN allowed for the supervised tuning of the initial linear transform's performance by gradient descent. DCT2net, a completely interpretable CNN, is born as a result.

A task-informed model training strategy that preserves task-specific information was developed by Kaiyan et al.,[23] and was established and thoroughly tested using clinically accurate simulated low-dose X-ray computed tomography (CT) images. Binary signal identification tasks are explicitly taken into account under signal-known-statistically (SKS) and background-known-statistically (BKS) conditions.

III. PROPOSED METHOD

3.1. Working Flow of Proposed HDCNN Model

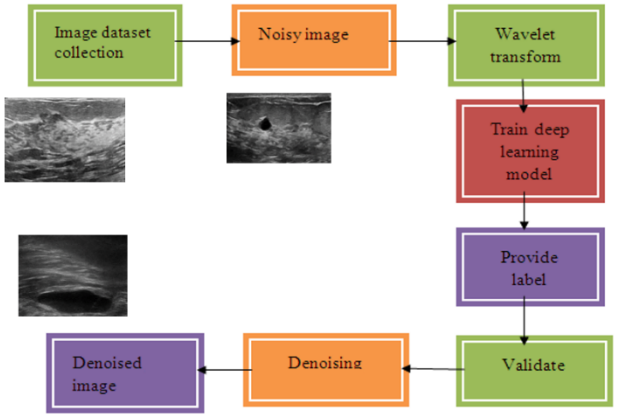

Figure1.Proposed workflow

The aforementioned model in Figure 1 illustrates the Deep Convolution Neural Network flow.

Applying the wavelets change, four sub-bands are produced from the input and clean label pictures.

- By contrasting the input and cleaning the label pictures in the wavelet domain, fourier leftover pictures are created, which are then employed fresh labelling.
- Using the recently transformed source and identify, the network is then instructed to identify functional relationships between various inputs and outputs. Each wavelet sub-band's four identical patches are utilized as the training set.
- Between the initial and ultimate phases, a network is made up of five components.
- Each module contains a ReLU, two batching normalizations, and layers of convolution.
- The two layers of the first stage are a convolution layer with ReLU and a convolution layer with regularization by batch and ReLU.
- The final phase consists of two convolutional layers, a terminal inversion layer, and a batch normalizing layer. A recurrent framework for learning to learn "R" and group normalization to quicken learning and improve blurring efficiency make up the two main parts of this technique.
- Now, we join all of the denoised patches together to form an entire image. Our hybrid method first divides the image into band frequencies utilizing wavelets, then trains mappings of features using a model based on deep learning to achieve inverse transform denoising.

International Journal on Recent and Innovation Trends in Computing and Communication
ISSN: 2321-8169 Volume: 11 Issue: 10
DOI: https://doi.org/10.17762/ijritcc.v11i10.8520
Article Received: *04 August 2023* ***Revised:*** *30 September 2023* ***Accepted:*** *15 October 2023*

3.2. Network Architecture

We suggest just one inversion and a 34-layer composite DnCNN with DB, RVB, and FB. To gather more contextual data, DB uses BN, common convolution, dilated convolutions, as including the triggering role of ReLU. For the purpose of extracting comparable breadth characteristics, RVB uses a parallel mixture of BN and ReLU. The RVB's refining characteristics are used to refine FB, which is then utilized to collect more precise data. To create a crisp image, just one inversion works in conjunction with a latent learning process. We employ an equation to offer the examples below in order to fully show the predicted HDCNN's method in Fig. 1:

$$I_c = HDCNN(I_n) = I_n - C(FB\left(RVB\left(DB(I_n)\right)\right)) \quad (1)$$

Ic and In, where HDCNN stands for the HDCNN algorithm, are a predicted pure picture and a supplied chaotic picture, respectively. DB, RVB, FB, and C, accordingly, express the parameters of DB, RVB, FB, and one volution.

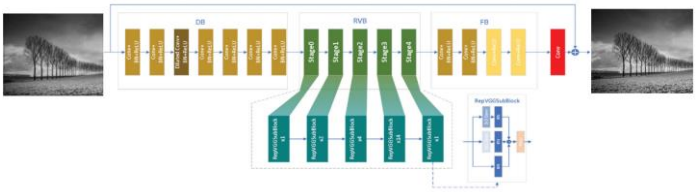

Figure2. Network architecture of the proposed HDCNN.

In order to manage pixel data, a specific type of neural association known as persuasive neural organization (CNN) is employed to recognize and respond to an evidently planned image. CNN takes into account a number of variables, including the ability to see clearly, computer-assisted (AI) imaging, which is employed either in person and online to make choices on a plan's structure and execution, as well as an understanding engine that contains videos and images for recommendation, NLP applauding and the manger's foundations.

Layers of neurons are coordinated to cover the entire area of study in order to avoid the challenge of preparing pictures utilizing normal neural connections. CNN uses a multi-part perceptron technique that seeks to cut down on administrative costs. The three types of layers that make up CNN are information, production, and a unique layer that incorporates various synchronization layers, blending layers, entirely integrated layers, and ordinary layers. The simpler path is only accessible to those aboard locomotives who are fascinated by regional languages and the processing of images due to constraints and more complete image exploitation methodologies.

CNN uses a multi-facet perceptron structure to lessen the amount of handling needed. The input layer, yield layer, and secret layer are components of the Neural sections, which additionally consist of multiple synchronization layers, mix layers, entirely coordinated sections, and normal levels. Building on classes that concentrated on image processing and language processing, a very effective, simple framework is created. Limitations are removed, picture handling skills are improved, and restrictions are lifted. Figure 2 illustrates the development of the Convolution Neural Network. The design of CNN has several layers and converts the information structure into a yield structure with divide ability. Typically, a variety of layers of various sorts are used.

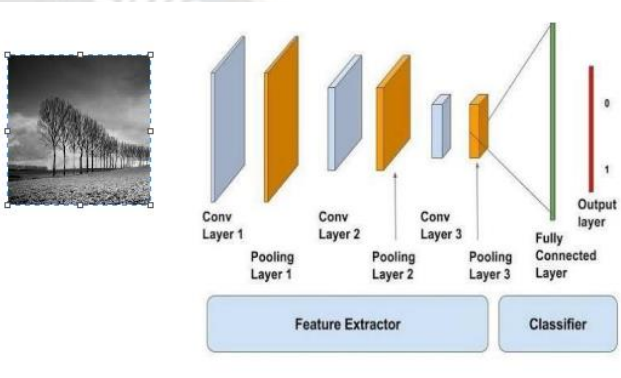

Figure3.CNN model

Convolutional Neural Networks (CNN) contain an array of levels, as shown in the diagram. The initial stage blends the decreased picture acquired from the color conversion program with the predetermined channels in order to estimate the impact of restricted correlation with likely roadway signal sites.

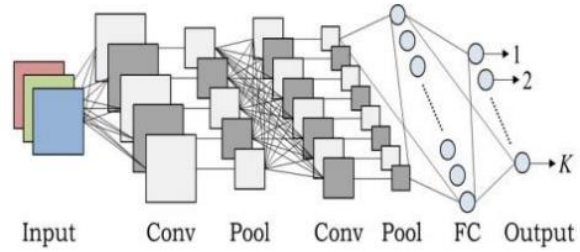

Figure4.Working of CNN layers

The multi-sided qualities of the separator are displayed in layers that are simple to comprehend in order to determine whether it belongs to the right class of traffic signals. These photos can be rotated without losing any of their quality. We only apply one channel to each category of restricting photographs due to their non-roundness. Hazardous channels are shown in Figure 3. The fact that pivot greatly impacts the arrangement of this section is the reason we need five channels to coordinate with one shape. Consistency with

International Journal on Recent and Innovation Trends in Computing and Communication
ISSN: 2321-8169 Volume: 11 Issue: 10
DOI: https://doi.org/10.17762/ijritcc.v11i10.8520
***Article Received:** 04 August 2023 **Revised:** 30 September 2023 **Accepted:** 15 October 2023*

the largest size is required because the photos traffic signs range in size from 16 x 16 to 128 x 128. We chose 1.05 as the value since it can give a satisfactory result in enough computer time.

It generates a full fix with a coefficient of contact greater than the breaking point for every unusual channel in each scale. We can produce a collection of fascinating locations by altering the restriction (ROI). There may be multiple ROIs located close to a single traffic signal because this estimate doesn't take into account distributed bundles. This problem was addressed by providing a simple ROI combination computation. The ROIs are organized by the coefficient of association with the slipping framework in each graph. The ROI with the highest value is selected as the positive district, and all other ROIs that are close to this location are prohibited. Repeat this progression until no more circuits are present.

3.3. Loss Function

Mean square error and loss function are training the HDCNN that is $\{I_i^n I_c^i\}$Cg, where $I_i^n$and I_c^i denote the ith noisy image and reference clean image, i = 1,2,3,4,….. N This can be explained as Eq. (2).

$$l(\theta) = \frac{1}{2N}\sum_{i=1}^{N}\left\|HDCNN(I_n^i) - I_c^i\right\| \quad (2)$$

Where θ is the parameter set and l is the loss function.

3.4. Enhanced Block

Deep architectures are recognized to be able to extract data with more accuracy, improving the performance of picture applications. Contextual contact can also improve a deep network's capacity for learning. This led to the creation of a 5-layer EB. A dilated convolution is used by EB to gather additional contextual data and improve SR performance. The resulting features are subsequently learned for picture denoising using three layered convolutional layers. The following list contains further details on EB.

Seven layers make up the EB, which are utilized to gather extra context data. Convolutional layer, BN, and ReLU are combined to form the first, second, fourth, fifth, sixth, and seventh layers, respectively. A dilated convolution, BN, and ReLU are included in the third layer, which is also written as dilated Conv+BN + ReLU. To gather more context data, the convolution is dilated. The training pace can be accelerated by BN. Linear characteristics are converted to nonlinearity using ReLU. The first layer's input and channel numbers are 3 and 64, respectively. Apart from the first layer, the DB's input and channel numbers are 64. All kernels are 3×3 in size. The aforementioned process can be displayed.

$$O_{DB} = DB(I_n)$$

$$=\text{RBC (RBC (RBC (RBDC (RBC (RBC }(I_n)))))) \quad (3)$$

3.5. Deformable Block

The 12-layer deformable block employs stacked convolutions and a malleable learnable kernel to provide more realistic noise features. Deformable Conv + ReLU, the first layer, stands for a deformable convolution and a ReLU activation function. To improve the quality of the predicted image, a deformable convolution exploits relationships between nearby pixels to reconstruct the position of the original pixel. The transformation of obtained linear features into non-linear features also uses ReLU. This layer has 3 and 64 input and output channels, respectively. In particular, the input channel for a given image is 1 if it is grey. Moreover, the kernel size is 3×3.

They have 64 input and output channels. Its kernel diameters are also 3 by 3. Data is normalized using BN to speed up the network. We define a few symbols in order to visually represent the aforementioned process. A deformable convolution and a ReLU are represented by the letters DC and R, respectively. Convolutional network (BN) functions are expressed, respectively, by C and B. RBC also stands for Conv + BN + ReLU.

$$O_{DB} = DB(I_n) = 11RBC(R(DC(In))) \quad (4)$$

Where O_{DB} is the output of DB, which is followed by an enhanced block.

Clarities of damaged images in image denoising can be improved by obtaining more precise contextual information. Strong geometric reshaping abilities of deformable convolution are utilized in this paper's network for picture denoising. Instead of the rigid rectangle kernel found in a standard convolution, it may learn from input and alter the position of each sampling point in a kernel.

Deformable convolution performs well in obtaining more contextual information, as shown by study of the aforementioned equations. Hence, we place a deformable convolutional layer, with parameters of input channel of 3, output channel of 64, and kernel size of 3×3, in front of the entire denoising process. The resulting linear features can then be transformed into non-linear features by a ReLU. Convolutional layer, BN, and ReLU are combined into a 12-layer model that is incorporated in the database in order to learn more precise features. The resulting features are

International Journal on Recent and Innovation Trends in Computing and Communication
ISSN: 2321-8169 Volume: 11 Issue: 10
DOI: https://doi.org/10.17762/ijritcc.v11i10.8520
***Article Received:** 04 August 2023 **Revised:** 30 September 2023 **Accepted:** 15 October 2023*

normalized using BN, and the resultant linear features are transformed into non-linearity using ReLU.

3.6. Repvgg Block

The 22-layer RVB obtains complimentary properties through a parallel method. Each of the 22 RepVGG subblocks in the parallel mechanism has three BN, three 33 Conv+BN, and one 11 Conv+BN routes. It has three output paths that can be combined using a residual procedure. A convolution layer combined with a 1×1 is known as 1×1 Conv+BN. There are 64 input and output channels across all tiers. The aforementioned explanation of the introduction is as follows:

$$O_{RVB} = RVB(O_{DB})$$

$$=22\text{RepVGGSubBlock}\ (O_{DB}) \quad (5)$$

$$RepVGGSubBlock(x) = R(B(x) + BC(x) + BC(x)) \quad (6)$$

Where 22RepVGG SubBlock denotes 22 stacked RepVGG subblocks. We assume that x is the input of RepVGG SubBlock.

3.7. Feature Refinement Block

To gather information that is more accurate, the 4-layer FB uses two types. The first kind, employed as the first and second layers in the feature refinement block, is Conv+BN + ReLU. The third and fourth layers in the feature refinement block are of the second type, Conv+ReLU. A convolution layer and ReLU are combined to form Conv+ReLU. Moreover, 64 is the channel number for their inputs and outputs. Their kernels are 3 by 3 in size. In Eq, the description can be displayed (7).

$$O_{FB} = FB(O_{RVB})$$

$$=\text{RB (RB (RCB (RCB }(O_{RVB}))))\quad (7)$$

3.8. Construction Clean Images

Clean images are created using a single convolution layer and a residual operation. The input and output channels are 64 and 3, respectively. The cited examples are as follows: Eq (8).

$$I_c = I_n - C(O_{FB}) \quad (8)$$

IV. PERFORMANCE MEASURES

The PSNR is calculated using the subsequent steps:

$$\text{Peak signal to noise ratio}=10\log_{10}\left(\frac{maximum_I^2}{mean\ square\ error}\right) \quad (9)\backslash$$

Here, $maximum_I^2$ is the highest value color image coordinates, and the mean square error is the deviation function of the image. Results from regional scattering elimination from sonar chest photos, as assessed by a boundary preservation value (BPI) When evaluating the recommended technique's estimation of nearby speckle disturbance annihilation in ultrasound pictures, the degree to which picture edges remain intact following eliminating noise must be taken into consideration in addition to the proportion of signal to noise and peak-to-average ratio. When assessing edge preservation achievement, a higher EPI value indicates a more trustworthy BPI. To explicitly determine EPI from experimental data, apply the following equation:

$$\text{Border protection index}= \frac{\sum_{i=0}^{n}(\nabla a-\Delta a)}{\sqrt{\sum_{i=0}^{n}(\nabla a-\nabla a)^2}} - \frac{\sum_{i=0}^{n}(\nabla b-\nabla b)}{\sqrt{\sum_{i=0}^{n}(\nabla b-\nabla b)^2}} \quad (10)$$

The relationship between the images before and after the ultrasound is described using the Laplace-operator, where a stands for the original image and b for the image with the localised speckle bruit removed. The improvement of image quality is inversely associated with the reduction in regional noise such as speckles in ultrasonic breast photos.

$$T_{des} = \sum_{k=1}^{m} t_{des}^{k} \quad (11)$$

The aforementioned procedure is employed for determining the period till annihilation. The efficient operation of regional scattering noise reduction in ultrasonic pictures of breasts is directly correlated with the quantity of time that is devoted to noise from images reduction following applying of multiple strategies.

V. EXPERIMENTAL RESULTS AND DISCUSSION

5.1. Datasets

For the MNIST database, 80000 grayscale images of breasts were downloaded from the internet. Both of them pieces of information consist of an initial set of 70000 images and an evaluation set of 12,000 images. For each set of ten digits, there are 7000 practice examples and 2000 test specimens. Images in this dataset are 2828 pixels wide.

To carry out an accurate evaluation of the effectiveness of the suggested models to those currently in use, a homogeneous experimental setting is needed. The DAE employed herein has 784 nodes that are input because the MNIST dataset's images are 2828 bytes in size and DAE can only be fed calibrated data. 784 neurons that provide input, 784 outputting brain cells, and 500 invisible neurons make up DAE. The DAE's input is a 2828 roughly directed chaotic picture, and its output is a 2828 linearly oriented raw image.

International Journal on Recent and Innovation Trends in Computing and Communication
ISSN: 2321-8169 Volume: 11 Issue: 10
DOI: https://doi.org/10.17762/ijritcc.v11i10.8520
***Article Received:** 04 August 2023 **Revised:** 30 September 2023 **Accepted:** 15 October 2023*

5.2. Experimental setup

This HDCNN has two layers, each of which has a convolution layer and a layer after it for sub sampling. The initialization of the kernels and other parameters is random. A 55 matrix is the filter that is used for the convolution task in both layers. The feature map is produced when the dot product is calculated for each place in the source image as this filter slides across it. The feature map is 2424 in size and has a depth of 6 due to the employment of 6 filters. Following that, each feature map is individually subjected to max pooling with a spatial neighborhood of a 2 by 2 window, increasing the feature map's size to 12 by 12.

It is followed by another convolution and pooling operation with the identical size cores and sharing area previously utilized, which decreases the dimensions of the map of features to 192 because the depth of the layer of convolution employed in this instance is 12. The final result of the second layer that pools resources serve as the input for the layer with full connection, which calculates the resulting chances for every class. The output layer of the HDCNN that was applied in this application has ten nodes.

To deal with image noise, every photo in the learning group has 20% unplanned corruption. In order to add turbulence to both the training and the testing picture specimens, an independent vector is started with the identical dimensions as the initial data set while a few of the cells inside the data are randomly turned OFF with a chance of 20%. Zero masking noise is the name of this approach. For testing purposes, 10%, 20%, and 50% of the data are initially switched on in three additional random matrices of the same size. These matrices are increased by the raw photos to produce the noisy images.

5.3. Result Discussion

A pair of ultrasound energy photos of breasts were used as the test subject. We reduced the preliminary picture to correspond to the corresponding imaging picture in a single pixel provided it into the HDCNN for incremental examinations, and observed the relationship between the square root of the error and incorrect accuracy of the graphic regional speckle signal detection as the number of cycles transformed. The average square error and incorrect identification frequencies of the HDCNN testing outcomes are shown in Table 1. Figure 5 displays a graphic representation of the HDCNN training results.

Figure5.HDCNN training outcome

Table1. HDCNN training results, both mean square error and false recognition rate

No.of iterations	MSE	FRV
1	1.4	0.7
2	1	0.5
3	0.8	0.4
4	0.7	0.3
5	0.4	0.2
6	0.3	0.1

Figure 6 displays the BPI range after the regional speckle disturbance has been eliminated. Figure 6 shows how the two states—before and following noise from speckles reduction—differ in terms of image quality. In both dataset's initial ultrasonic chest images, as shown in Figure 7, there were a number of local speckles that could have misinterpreted the state of the breast and possibly prevented the detection of small lesions.

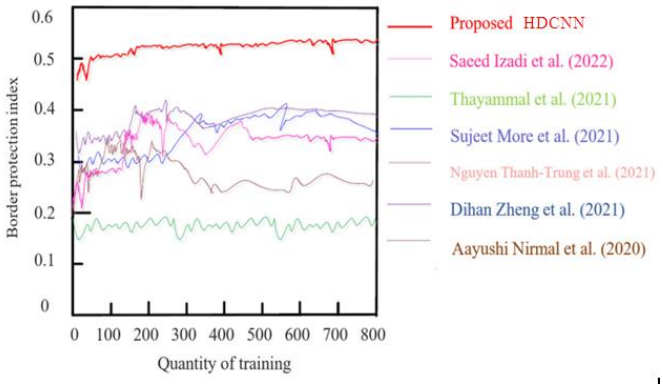

Figure6. BPI after local speckle noise-removal

International Journal on Recent and Innovation Trends in Computing and Communication
ISSN: 2321-8169 Volume: 11 Issue: 10
DOI: https://doi.org/10.17762/ijritcc.v11i10.8520
Article Received: *04 August 2023* ***Revised:*** *30 September 2023* ***Accepted:*** *15 October 2023*

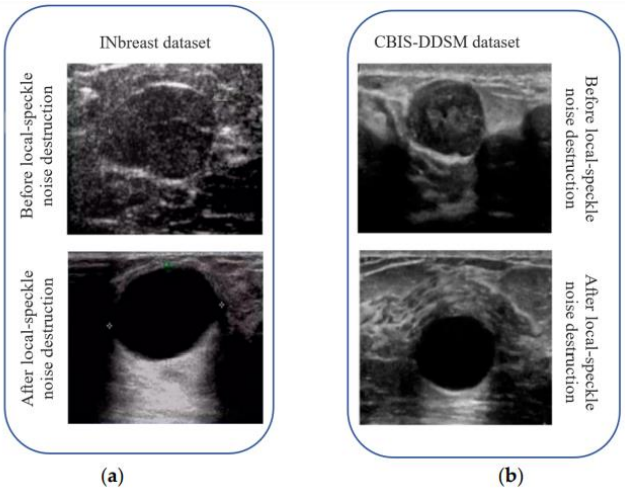

Figure7. INbreast and CBIS-DDSM dataset image comparison (a) before and after the destruction; (b) before and after the local speckle destruction.

This demonstrates that the suggested technique effectively gets rid of regional speckle interference from ultrasonography pictures of breasts without obliterating any significant data. On the basis of PSNR plus the quantity of period required to examine the data, the results of the denoising techniques were assessed.

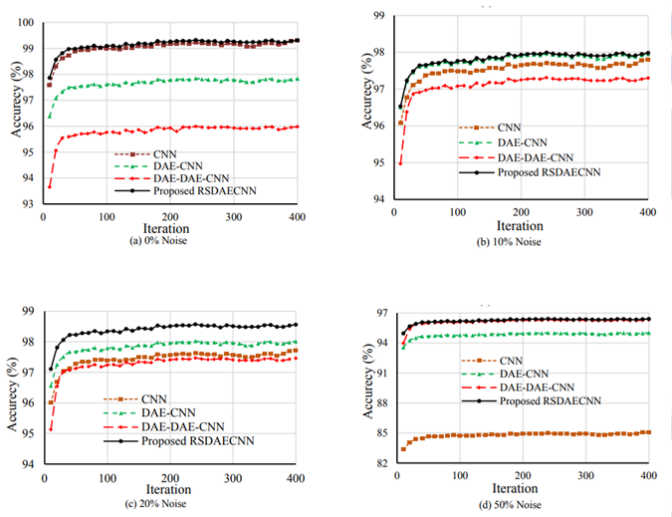

Figure8. Test set recognition accuracy with different noise levels.

The structure using CNN alone outperformed the other two separate structures, having the maximum classification accuracy of 99.31% for 0% noise (Fig. 8(a)). However, DAE-CNN and DAE-DAE-CNN had classification accuracy rates of 98.89% and 95.93%, respectively. These two models perform badly when compared to CNN alone due to CNN's training on silent native images. When an absence of noise picture is fed to a DAE that has been trained on 20% noise photographs, the DAE will try to change the contour of the picture to another form since it thinks the image has been tainted by 20% disturbance and will output an image that is distorting as a result. Utilizing cascaded DAE makes the situation worse.

So, it makes sense that DAECNN and DAE-DAE-CNN perform worse than a single CNN. The suggested model, however, outperforms these two models and is on par with a single CNN in terms of classification accuracy since it uses a winner-takes-all approach for the final class label selection. Because DAE is trained with 20% noise level, DAE-CNN is proved to be the most suitable individual structure for 10% noise (Fig. 8(b)). The performance of the suggested approach in this scenario is same to DAE-CNN. At 20% noise, DAE-CNN is shown to be the best individual structure (Fig. 8(c)), but curiously, the suggested model outperformed DAE-CNN in this situation.

On the other hand, in the case of 50% noise, DAE-DAE-CNN performed better than CNN and DAE-CNN. The reason why cascaded DAEs outperform single DAEs in circumstances of photos with extreme noise is already established because they are both trained at a 20% noise level. When the second DAE processes a noisy image from the first one, it receives a comparatively less noisy image that is further denoised. In such a case of extreme noise, the proposed technique showed comparable performance to DAEDAE-CNN. When all potential outcomes are considered, the suggested model performs well in noiseless to severe noise conditions.

The results of these tests are shown in Table 2. The list of short forms and their corresponding abbreviations are described by the word abbreviation. The noise removal comparison chart with a graphical representation of proposed and cutting-edge technologies is shown in Figure 9. Table 2 demonstrates that the suggested method outperforms the previous techniques in terms of peak and overall noise when white Gaussian noise is applied to the INbreast and DDSM datasets at varied levels. The suggested approach offers improved local speckle noise reduction and lower noise sensitivity.

Table 2. Image noise removal comparison chart of proposed and state-of-art methods

Methods	**INbreast Dataset**			**CBIS-DDSM Dataset**		
	25dB	**45dB**	**65Db**	**25dB**	**45Db**	**65dB**
Saeed Izadi et al. (2022)	12	19	16	16	17	17
Thayammal et al. (2021)	20	17	19	18	13	18
Sujeet More et al. (2021)	14	15	23	19	15	13

International Journal on Recent and Innovation Trends in Computing and Communication
ISSN: 2321-8169 Volume: 11 Issue: 10
DOI: https://doi.org/10.17762/ijritcc.v11i10.8520
***Article Received:** 04 August 2023 **Revised:** 30 September 2023 **Accepted:** 15 October 2023*

Nguyen Thanh-Trung et al. (2021)	17	18	25	12	19	12
Dihan Zheng et al. (2021)	12	10	18	23	20	19
shi Nirmal et al. (2020) [9	10	16	16	25	17	20
HDCNN	6	9	10	11	15	13

Figure9. Graphical view of image noise removal comparison chart of proposed and state-of-art methods

This clearly shows that the suggested method visualizes ultrasound breast images well while reducing local speckle noise without sacrificing edge information.

Table 3. Image noise removal state-of-art method

Methods	SNR (dB)	PSNR (dB)
Saeed Izadi et al. (2022)	58.2	65.9
Thayammal et al. (2021)	57.1	64.2
Sujeet More et al. (2021)	59.3	67.2
Nguyen Thanh-Trung et al. (2021)	56.3	66.8
Dihan Zheng et al. (2021)	57.4	63.7
Aayushi Nirmal et al. (2020)	56.2	64.1
Proposed HDCNN	62.6	68.7

The experimental object was a random selection of sonar images of the breast from the two data sets, and the recommended technique was utilized to conduct local speckle noise destruction tests to assess the relative SNR and peak SNR. This shows that the proposed approach reduces noise from breast ultrasound images more efficiently than state-of-the-art techniques. The recommended method was evaluated using a collection of sonar pictures of breasts with a BPI limit of 0.45, and outcomes came from a statistical evaluation of the EPI values that were generated following suppression. Piezo electric material eigen frequencies are implemented in Paper [26].

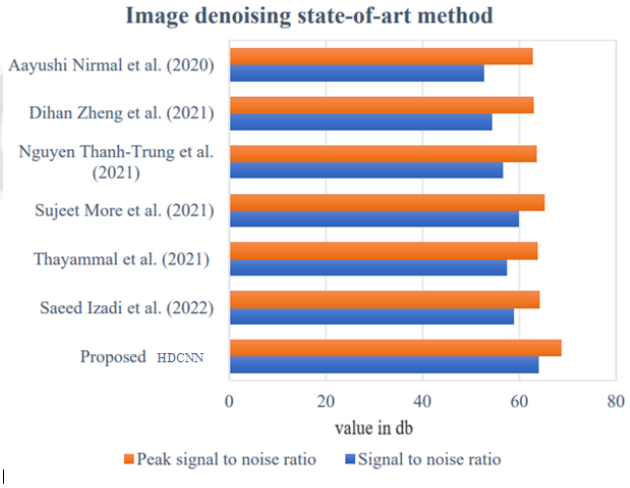

Figure10. Graphical view of image noise removal different state-of-art-method

VI. CONCLUSION

Given the circumstances of actual life, noisy visual data is typical. With the aid of the currently used classification techniques, pre-processed noiseless photos can be categorized with simplicity. A supervised classifier, however, finds it challenging to deal with the noisy data that is directly provided to it, and classification failure is almost a guarantee. In this study, auto encoders are used to rebuild the image from its noisy version before sending the updated image to a classifier. The fact that it is impossible to tell in advance how much noise is carried by image data is another crucial factor. A novel model that incorporates HDCNN is studied in light of all these details. This model eliminates the need to train it for various noise levels. Due to its noise independence, the proposed model outperformed previous models on the MNIST dataset when it came to categorizing images with noise levels ranging from zero to large, proving that it is capable of learning hierarchical representations.

Authors Contribution

First two authors involved in data collection and 3 and 4th authors involved simulation works and 5th author wrote the manuscript and prepared the figure. Also, all authors reviewed the manuscript.

International Journal on Recent and Innovation Trends in Computing and Communication
ISSN: 2321-8169 Volume: 11 Issue: 10
DOI: https://doi.org/10.17762/ijritcc.v11i10.8520
***Article Received:** 04 August 2023 **Revised:** 30 September 2023 **Accepted:** 15 October 2023*

Conflict of Interest and Authorship Conformation Form

- All authors have participated in (a) conception and design, or analysis and interpretation of the data; (b) drafting the article or revising it critically for important intellectual content; and (c) approval of the final version.
- The authors have no affiliation with any organization with a direct or indirect financial interest in the subject matter discussed in the manuscript

References

[1] Kang, Yanqin, et al. "Denoising Low-Dose CT Images Using a Multi-Layer Convolutional Analysis-Based Sparse Encoder Network." 2022 15th International Congress on Image and Signal Processing, BioMedical Engineering and Informatics (CISP-BMEI). IEEE, 2022.

[2] Takeyama, Saori, and Shunsuke Ono. "Robust Hyperspectral Image Fusion with Simultaneous Guide Image Denoising via Constrained Convex Optimization." IEEE Transactions on Geoscience and Remote Sensing 60 (2022): 1-18.

[3] Wang, Zhicheng, et al. "Nonlocal self-similarity-based hyperspectral remote sensing image denoising with 3-d convolutional neural network." IEEE Transactions on Geoscience and Remote Sensing 60 (2022): 1-17.

[4] Singh, Prabhishek, et al. "A Method Noise-Based Convolutional Neural Network Technique for CT Image Denoising." Electronics 11.21 (2022): 3535.

[5] Yang, Haibo, et al. "Denoising of 3D MR images using a voxel-wise hybrid residual MLP-CNN model to improve small lesion diagnostic confidence." Medical Image Computing and Computer Assisted Intervention–MICCAI 2022: 25th International Conference, Singapore, September 18–22, 2022, Proceedings, Part III. Cham: Springer Nature Switzerland, 2022.

[6] Wang, Jiachen, Yingyun Yang, and Yan Hua. "Image quality enhancement using hybrid attention networks." IET Image Processing 16.2 (2022): 521-534.

[7] Madhura, D. M., and AV Krishna Mohan. "Hybrid Image Denoising with Wavelet and Deep Learning Model." Journal of Pharmaceutical Negative Results (2022): 1282-1288.

[8] Chen, Hongyu, Guangyi Yang, and Hongyan Zhang. "Hider: A hyperspectral image denoising transformer with spatial–spectral constraints for hybrid noise removal." IEEE Transactions on Neural Networks and Learning Systems (2022).

[9] Zhao, Mo, et al. "Hybrid Transformer-CNN for Real Image Denoising." IEEE Signal Processing Letters 29 (2022): 1252-1256.

[10] Zheng, Menghua, et al. "A hybrid CNN for image denoising." Journal of Artificial Intelligence and Technology 2.3 (2022): 93-99.

[11] Kang, Yanqin, et al. "Denoising Low-Dose CT Images Using a Multi-Layer Convolutional Analysis-Based Sparse Encoder Network." 2022 15th International Congress on Image and Signal Processing, BioMedical Engineering and Informatics (CISP-BMEI). IEEE, 2022.

[12] Atal, Dinesh Kumar. "Optimal Deep CNN–Based Vectorial Variation Filter for Medical Image Denoising." Journal of Digital Imaging (2023): 1-21.

[13] Praveena, Hirald Dwaraka, et al. "Effective CBMIR System Using Hybrid Features-Based Independent Condensed Nearest Neighbor Model." Journal of Healthcare Engineering 2022 (2022).

[14] Guo, Shuli, et al. "COVID-19 CT image denoising algorithm based on adaptive threshold and optimized weighted median filter." Biomedical Signal Processing and Control 75 (2022): 103552.

[15] Balamurugan, T., and E. Gnanamanoharan. "Brain tumor segmentation and classification using hybrid deep CNN with LuNetClassifier." Neural Computing and Applications 35.6 (2023): 4739-4753.

[16] Kim, Dai-Gyoung, et al. "Hybrid deep learning framework for reduction of mixed noise via low rank noise estimation." IEEE Access 10 (2022): 46738-46752.

[17] Herbreteau, Sébastien, and Charles Kervrann. "DCT2net: an interpretable shallow CNN for image denoising." IEEE Transactions on Image Processing 31 (2022): 4292-4305.

[18] Vimala, Baiju Babu, et al. "Image Noise Removal in Ultrasound Breast Images Based on Hybrid Deep Learning Technique." Sensors 23.3 (2023): 1167.

[19] Reddy, C. Kishore, et al. "A Review of Image Denoising using Machine Learning." Futuristic Sustainable Energy and Technology (2022): 281-290.

[20] Acar, Vedat, and Ender M. Eksioglu. "Densely Connected Dilated Residual Network for Image Denoising: DDR-Net." Neural Processing Letters (2022): 1-15.

[21] Yuan, Yu, et al. "Ghost-free High Dynamic Range Imaging via Hybrid CNN-Transformer and Structure Tensor." arXiv preprint arXiv:2212.00595 (2022).

[22] Tuncer, Seda Arslan, and Ahmet Alkan. "Classification of EMG signals taken from arm with hybrid CNN-SVM architecture." Concurrency and Computation: Practice and Experience 34.5 (2022): e6746.

[23] Thakur, Rini Smita, et al. "Medical image denoising using convolutional neural networks." Digital Image Enhancement and Reconstruction. Academic Press, 2023. 115-138.

[24] Yancheng, L. I., et al. "RED-MAM: A residual encoder-decoder network based on multi-attention fusion for ultrasound image denoising." Biomedical Signal Processing and Control 79 (2023): 104062.

[25] Mukilan, P., and Wogderess Semunigus. "Human and object detection using hybrid deep convolutional neural network." Signal, Image and Video Processing 16.7 (2022): 1913-1923.

[26] Sivakumar, N., Kanagasabapathy, H., Srikanth, H. P., Amuthan, N." Eigen Frequencies Analysis of Pre-Charged and Uncharged Piezoelectric Microcantilevers Beams", Advanced Science, Engineering and Medicine, Volume 11, Number 6, June 2019, pp. 491-498(8), American Scientific Publishers, https://doi.org/10.1166/asem.2019.2380